2014

Kinetic modeling of evolution of 3 + 1:Resonance enhanced multiphoton ionization plasma in argon at low pressures

Siva Sashank Tholeti
Purdue University

Mikhail N. Shneider
Princeton University

Alina A. Alexeenko
Purdue University - Main Campus, alexeenk@purdue.edu

Kinetic modeling of evolution of 3+1:Resonance enhanced multiphoton ionization plasma in argon at low pressures

Siva Sashank Tholeti, Mikhail N. Shneider, and Alina A. Alexeenko

Citation: Physics of Plasmas **21**, 063507 (2014); doi: 10.1063/1.4882261
View online: http://dx.doi.org/10.1063/1.4882261
View Table of Contents: http://scitation.aip.org/content/aip/journal/pop/21/6?ver=pdfcov
Published by the AIP Publishing

Kinetic modeling of evolution of 3 + 1:Resonance enhanced multiphoton ionization plasma in argon at low pressures

Siva Sashank Tholeti,[1] Mikhail N. Shneider,[2] and Alina A. Alexeenko[1,a)]
[1]School of Aeronautics and Astronautics, Purdue University, West Lafayette, Indiana 47907, USA
[2]Mechanical and Aerospace Engineering, Princeton University, Princeton, New Jersey 08544, USA

(Received 1 April 2014; accepted 26 May 2014; published online 16 June 2014)

We present numerical kinetic modeling of generation and evolution of the plasma produced as a result of resonance enhanced multiphoton ionization (REMPI) in Argon gas. The particle-in-cell/Monte Carlo collision (PIC/MCC) simulations capture non-equilibrium effects in REMPI plasma expansion by considering the major collisional processes at the microscopic level: elastic scattering, electron impact ionization, ion charge exchange, and recombination and quenching for metastable excited atoms. The conditions in one-dimensional (1D) and two-dimensional (2D) formulations correspond to known experiments in Argon at a pressure of 5 Torr. The 1D PIC/MCC calculations are compared with the published results of local drift-diffusion model, obtained for the same conditions. It is shown that the PIC/MCC and diffusion-drift models are in qualitative and in reasonable quantitative agreement during the ambipolar expansion stage, whereas significant non-equilibrium exists during the first few 10 s of nanoseconds. 2D effects are important in the REMPI plasma expansion. The 2D PIC/MCC calculations produce significantly lower peak electron densities as compared to 1D and show a better agreement with experimentally measured microwave radiation scattering. © *2014 AIP Publishing LLC*. [http://dx.doi.org/10.1063/1.4882261]

I. INTRODUCTION

There is a great interest for studying plasma and its applications, generated as a result of Resonance Enhanced Multiphoton Ionization (REMPI). Primarily, due to the use of REMPI in a recently appeared precise non-perturbative diagnostics,[1] as well as for pre-ionization in plasma-assisted ignition methods.[2]

In the papers,[3–5] the evolution of laser-induced REMPI plasma was modeled within the framework of nonstationary one-dimensional (1D) drift-diffusion approximation, in which the electron temperature is determined by the heat conduction equation. This approximation is valid for the equilibrium Maxwellian electron gas. It should be expected that a more adequate approach to describe the REMPI plasma is non-local, due to its small dimensions (~10–100 μm) and the short formation time (~1–100 ns). This is determined by the focusing area and a pulse duration of the laser beam and a relatively small lifetime of the plasma due to its expansion and recombination decay. A natural question arises, how great is the error of the local drift-diffusion approximation and how adequate is it for the description of experiments. In this paper, we performed the numerical modeling of the REMPI plasma evolution using Particle-In-Cell method with Monte Carlo Collisions (PIC/MCC) at experimental conditions[4] and the results are compared with calculations based on the local drift-diffusion approximation and experiments for the same conditions.

Nonlocal effects become more pronounced with decreasing gas pressure. Therefore, PIC/MCC calculations in this paper were performed for REMPI plasma in Argon for the lowest pressure p = 5 Torr, at which the experiments were conducted,[4] and compared with calculations performed in the framework of drift-diffusion approximation for the same experimental conditions.[4]

The remainder of the paper is organized as follows. Section II details the numerical method and physical models with simulation setup explained in Sec. III. Results of 1D and two-dimensional (2D) PIC/MCC simulations are presented in Sec. IV and compared with 1D drift-diffusion model as well as experimental data.

II. NUMERICAL MODEL

Unlike continuum fluid approximations of plasma dynamics, kinetic models capture non-equilibrium transport and relaxation/excitation processes. These non-equilibrium processes are important when a characteristic time/length scales of the problem are comparable to time/length scales of the microscopic motion of a charged species. The minimum length scale of REMPI plasma considered by Shneider *et al.*[3] is 10 μm and the mean free path of Ar gas at 5 Torr at 300 K is approximately 8 μm, this indicates a Knudsen number, Kn = 0.8, i.e., the rarefied gas flow regime. Additionally, the time scale of the expansion process and the laser pulse is in nano-seconds, while the time taken by the electrons at 3.2 eV to equilibrate is ≈3 μs. Thus non-equilibrium effects are expected to be significant. In order to study the energy distribution of electrons and for a more accurate prediction of number density as compared to the fluid model, PIC/MCC[6] method has been chosen. In general, PIC/MCC method solves the fundamental kinetic equations of Boltzmann without equilibrium approximation.

Particles are defined in continuum space through their position and velocity. Field is determined at discrete

a)Electronic mail: alexeenk@purdue.edu.

locations in space. However, both fields and particles are defined at discrete times. Particle and field values are advanced sequentially in time, starting from initial conditions, with a temporal leap-frog scheme.[10] Monte Carlo Collision scheme is applied to consider collisions. A schematic of PIC/MCC simulation algorithm for REMPI plasma expansion is shown in Fig. 1. In the Lorenz force, the component due to magnetic field is negligible in comparison with that due to electric field in the present case and, hence, not considered in the computations. The electric field is computed from the electric potential, which in turn is computed by solving the Poisson equation using Dynamic Alternating Direction Implicit (DADI) numerical scheme which is unconditionally stable.[15]

Since low pressure REMPI plasma in Ar is considered, the major species (with Ar as the background gas) involved in the process are electrons, Ar ions (Ar^+) and Ar metastables (Ar^*). The molecular ions are neglected for the low-pressure case of $p = 5$ Torr. The generation of metastables, electrons, and ions is based on the total photon flux from the laser pulse, which is integrated in time to obtain net flux during the time step and is performed before the particles are weighted to the grid at the beginning of every time step as shown in Fig. 1.

The fundamental kinetic equation of Boltzmann for each species in this case can be written as

$$\frac{\partial(f_* n_*)}{\partial t} + \mathbf{v}_* \cdot \frac{\partial(f_* n_*)}{\partial \mathbf{r}} = C_* + \dot{n}_*^{REMPI} f_*^M, \tag{1}$$

$$\frac{\partial(f_e n_e)}{\partial t} + \mathbf{v_e} \cdot \frac{\partial(f_e n_e)}{\partial \mathbf{r}} + \frac{q_e \mathbf{E}}{m_e} \cdot \frac{\partial(f_e n_e)}{\partial \mathbf{v_e}} = C_e + \dot{n}_e^{REMPI} f_e^{RI}, \tag{2}$$

$$\frac{\partial(f_+ n_+)}{\partial t} + \mathbf{v}_+ \cdot \frac{\partial(f_+ n_+)}{\partial \mathbf{r}} - \frac{q_e \mathbf{E}}{m_+} \cdot \frac{\partial(f_+ n_+)}{\partial \mathbf{v}_+} = C_+ + \dot{n}_+^{REMPI} f_+^{RI}. \tag{3}$$

The terms C, n, f, and $\mathbf{v}$ are the collision integral, number density, velocity distribution function, and relative velocity, respectively. The subscripts "*", "e," and "+" represent metastables, electrons, and atomic ions, respectively, with q_e being the charge of an electron. The metastable relaxation term C_* consists of the quenching reactions with neutrals, i.e., binary and three body quenching and time decay. The collision term for electrons, C_e, includes the ionization of neutrals, recombination with ions and binary elastic collisions with neutrals. The ion collision term, C_+, consists of the ionization of neutrals, charge exchange collisions, recombination with electrons and binary elastic collisions with neutrals.

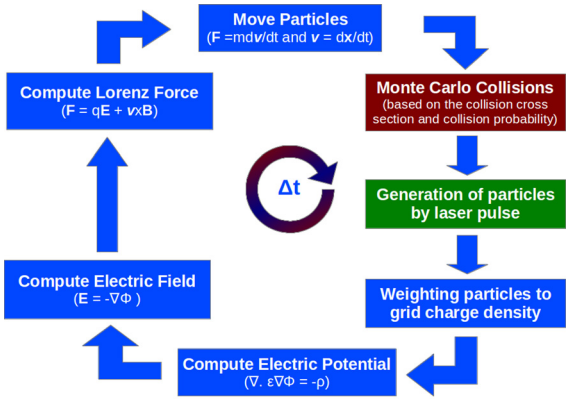

FIG. 1. PIC/MCC algorithm.

The particles generated by the REMPI process are modeled as source terms for each species, as given in the last term of Eqs. (1)–(3). The term f^M represents Maxwellian velocity distribution function with 0.026 eV as the mean energy, and f^{RI} is the random isotropic velocity distribution function with a constant energy, which is 3.2 eV in case of electrons and 0.026 eV in case of ions. The parameters σ, β_{eff}, k_1, and k_2 are the collision cross-section, effective recombination rate coefficient of Argon ion and electron, binary quenching rate coefficient and three body quenching rate coefficient for Ar^*, respectively. The net rate of number density change of a species due to excitation or ionization by REMPI is given by $\dot{n}^{REMPI}$. The effective life-time of Ar metastables is $\tau_d = 66$ ns. The reactions involved in the REMPI plasma expansion process in Ar gas are listed in Table I. Figure 2 shows the dependence of collision cross section on energy for electron-neutral collisions and ion-neutral collisions.

A. Model for particle generation by REMPI

The three photon excitation cross section, $\sigma_{(3)} = 2.81 \times 10^{-92}\,\mathrm{m^6\,s^2}$ and single photon ionization cross section, $\sigma_{Pi} = 7.77 \times 10^{-23}\ \mathrm{m^2}$ have been used for 3 + 1:REMPI of Argon, which have been calculated by Zhang *et al.*[3] The number of metastables (N_*), electrons (N_e), and ions (N_+) to be generated in a volume ΔV at the $(i+1)$th time step (with "i" being the previous time step number) due to REMPI, are based on the total photon flux and the gas number density, n_g and metastable number density, n_* (since $\dot{n}^{REMPI} = limit_{\Delta t \to 0, \Delta V \to 0} N/(\Delta V \Delta t)$) and are given by

$$\begin{aligned} N_*^{i+1} &= \Delta V (n_g \sigma_{(3)} (F^{i+1})^3 - n_*^i \sigma_{Pi} F^{i+1}), \\ N_e^{i+1} &= \Delta V (n_*^{i+1} \sigma_{Pi} F^{i+1}), \\ N_+^{i+1} &= \Delta V (n_*^{i+1} \sigma_{Pi} F^{i+1}). \end{aligned} \tag{4}$$

The time dependence of laser pulse is shown in Fig. 3. The total photon flux over time can be computed either by analytically integrating the photon flux in the time between the time limits or by multiplying the volume average of photon flux with the time step (given by the time between the limits used in integration). However, the latter approach over predicts by 1%, which is significant when the number of particles being generated are almost in the order of millions and hence the former method is used in the present model. The time integrated total photon flux, F, is a function of the laser pulse frequency, ω (for a wavelength of 261.27 nm), and the laser pulse intensity, I, and is given by

$$F^{i+1} = \int_{t^i}^{t^{i+1}} \frac{I(r,z,t)}{\hbar\omega} dt, \tag{5}$$

where $\hbar$ is the reduced Plank's constant. Laser intensity, which is given by

TABLE I. Collisions modeled in PIC/MCC simulations for Argon gas.

S. No	Type of collision	Collision	Rate coefficients[7–9]/cross sections[10]
(1)	Electron elastic	$Ar + e \rightarrow Ar + e$	$\sigma(m^2) = \begin{cases} \frac{1}{10\left(19+\frac{\epsilon}{0.11}\right)}, \epsilon \le 0.2\,\text{eV} \\ \frac{(9.07\times10^{-19})\epsilon^{1.55}(\epsilon+70)^{1.1}}{(1.4+\epsilon)^{3.25}}, \epsilon > 0.2\,\text{eV} \end{cases}$
(2)	Impact ionization	$Ar + e \rightarrow Ar^+ + 2e$	$\sigma(m^2) = \begin{cases} \frac{1.7155\times10^{-18}(\epsilon-15.76)}{\epsilon^2 ln(0.0634\epsilon)}, 15.76\,\text{eV} \le \epsilon \le 79\,\text{eV} \\ \frac{2.648\times10^{-18}(\epsilon-15.76)}{\epsilon^2 ln(0.0344\epsilon)}, \epsilon > 79\,\text{eV} \end{cases}$
(3)	Ion elastic	$Ar + Ar^+ \rightarrow Ar + Ar^+$	$\sigma(m^2) = 1.8\times10^{-19} + \frac{4\times10^{-19}}{\sqrt{\epsilon}}, \epsilon \ge 4\,\text{eV}$
(4)	Charge exchange	$Ar + Ar^+ \rightarrow Ar^+ + Ar$	$\sigma(m^2) = 2\times10^{-19} + \frac{5.5\times10^{-19}}{\sqrt{\epsilon}}, \epsilon \ge 4\,\text{eV}$
(5)	Binary quenching	$Ar^* + Ar \rightarrow Ar + Ar$	$k_1 = 10^{-21}$ [m^3/s]
(6)	Three body quenching	$Ar^* + 2Ar \rightarrow Ar + 2Ar$	$k_2 = 10^{-34}$ [m^6/s]
(7)	Recombination	$Ar^+ + 2e \rightarrow Ar + e$	For $T_e < 0.5$ eV, $\beta_{eff} = 1.55\times10^{-16}T_e^{-0.63} + 3.61\times10^{-17}T_e^{-2.18}n_e^{0.37} + 3.8\times10^{-21}T_e^{-4.5}n_e$[m^3/s] ($T_e$ in K and n_e in m^{-3}) For $T_e \ge 0.5$ eV, $\beta_{eff} = 8.75\times10^{-39}T_e^{-4.5}n_e + 2.9\times10^{-19}T_e^{-0.75}$[m^3/s] ($T_e$ in eV and n_e in m^{-3})

$$I = I_0 \exp\left[-\left(\frac{2(t-t_0)}{\tau_p}\right)^2 - \left(\frac{r}{r_b}\right)^2 - \left(\frac{z}{z_b}\right)^2\right], \quad (6)$$

where, $I_0 = 2E/(\pi^{3/2}r_b^2\tau_p)$ is the amplitude of the intensity, E is the energy of the pulse, τ_p is the full-width half maximum of the pulse, r_b is the laser focal radius, and z_b is the axial focal length. The full kinetic computation of gas heating involves the computation of exact energy loss by plasma to the neutrals in every collision and coupling it to Boltzmann equation for the gas to solve for the microscopic thermal distribution.

B. Model for collisional processes

With ions as the target species in the recombination collisions, the frequency of effective recombination of Argon ions with electrons is $\nu_{eff}(r,z,T_e) = \beta_{eff}(r,z,T_e)n_+(r,z)$. Hence, the probability of an electron undergoing effective recombination in a time Δt is $P_{eff} = 1 - \exp(-\nu_{eff}(r,z,T_e)\Delta t)$. The electron undergoing collision is chosen randomly, and the collision takes place if the uniform random number generated is less than P_{eff}.

The loss of metastables to neutral atoms occurs by binary quenching, three body quenching, and time decay. Let the frequency of these loss mechanisms be ν_1, ν_2, and ν_3, respectively, which are functions of spatial coordinates (r, z) and energy of metastables. These processes are modeled by the null collision method.[10] The null collision frequency is given by, $\nu' = max_{r,z,\varepsilon}(\nu_1 + \nu_2 + \nu_3)$. Hence, the maximum number of metastables that undergo the loss processes in a time Δt is given by $N_*(1 - \exp(-\nu'\Delta t))$. The metastables undergoing collisions are chosen randomly and the mechanism of loss process of a metastable with energy ε_* is determined with the help of a random number, R as given in Eq. (7)

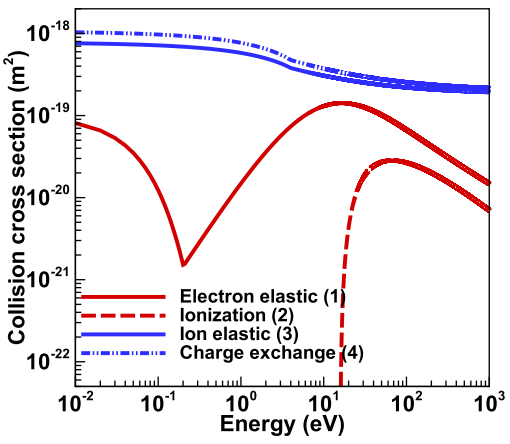

FIG. 2. Collision cross-sections for neutral interaction with electrons and ions in Ar gas.[10]

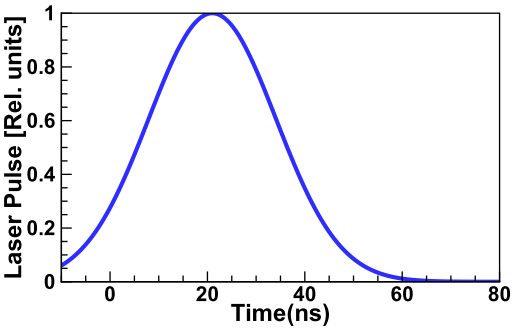

FIG. 3. Laser pulse in time domain used in experiments.[4]

$$
\begin{aligned}
R &\le \frac{\nu_1(\varepsilon_*)}{\nu'} \\
&\Rightarrow \text{Binary quenching} \\
\frac{\nu_1(\varepsilon_*)}{\nu'} < R &\le \frac{\nu_1(\varepsilon_*) + \nu_2(\varepsilon_*)}{\nu'} \\
&\Rightarrow \text{Three body} \\
&\quad \text{quenching} \\
\frac{\nu_1(\varepsilon_*) + \nu_2(\varepsilon_*)}{\nu'} < R &\le \frac{\nu_1(\varepsilon_*) + \nu_2(\varepsilon_*) + \nu_3(\varepsilon_*)}{\nu'} \\
&\Rightarrow \text{Time decay} \\
\frac{\nu_1(\varepsilon_*) + \nu_2(\varepsilon_*) + \nu_3(\varepsilon_*)}{\nu'} < R &\Rightarrow \text{No collision.}
\end{aligned} \tag{7}
$$

III. SIMULATION SETUP

This section gives a brief description of the parameters and the boundary conditions considered for the simulations. All simulations were performed in cylindrical co-ordinate system, since the problem is axisymmetric. For 1D and 2D simulations, all the boundaries except the axis (for 1D simulations, boundaries are only in the radial direction) were considered to be at a potential of 0 V. The initial electron energy considered in the simulation is based on a random isotropic velocity distribution,[16] with constant energy of 3.2 eV, across all the electrons generated from the laser pulse. Both 1D and 2D PIC/MCC simulations[11] were performed at a gas pressure of 5 Torr and a gas temperature of 300 K.

The constraint on the grid size is to resolve the smallest characteristic length scale of plasma, i.e., Debye length, hence a grid size of 0.5 μm was used both in radial and axial directions. The constraint on time-step is that it should be small enough that the fastest moving particle, i.e., the electron, does not cross more than one cell in a given time-step and hence a time step of 10^{-13} s was used in all the simulations. The REMPI plasma is simulated in 1D with 512 cells in the radial direction and a total of about 0.5×10^6 computational particles. The 2D simulations are performed with over 600 cells in the axial direction and 500 cells in the radial direction and about 1×10^6 particles ensemble averaged over 5 simulations with varying random seed values.

IV. RESULTS AND DISCUSSION

The results presented here are from the PIC/MCC simulations for the 3 + 1:REMPI of Argon at 5 Torr and at a temperature of 300 K, with respect to the experimental laser pulse parameters:[4] energy per pulse, $E = 2.1$ mJ/pulse, $\tau_p = 37$ ns, effective beam radius, $r_b = 7.5$ μm; effective beam axial length, $z_b = 100$ μm; laser wavelength = 261.27 nm. The laser is assumed to start at t = −10 ns. The results are plotted considering $R = 2$ μm, which is 4 cells away from the axis, as near the axis. This is done for better statistical accuracy in comparison with $R = 0.5$ μm, which is only one cell away from the axis, because of the square dependence of the volume on the radius.

A. 1D approximation

The radial distribution of number densities of all the species considered at 0 ns and 50 ns are shown in Fig. 4. The evolution of the radial distribution of number densities of ions and electrons in Fig. 4, indicates ambipolar diffusion of plasma. The electrons out of the quasi-neutral region in Figs. 4(a) and 4(b) are the electrons that have initially diffused through free diffusion and those that have escaped the polarization field.

A comparison of radial number density distribution of electrons, ions, and metastables at 100 ns from PIC/MCC simulation and fluid approximation calculations from Shneider *et al.*[4] is shown in Fig. 5. Ambipolar diffusion along with free diffusion outside the bounds of the quasi-neutral plasma can be seen in Fig. 5. A good agreement has been found with respect to number density distribution and also the boundary of the quasi-neutral region at 100 ns with the results from Shneider *et al.*[4] There is a difference in the number density distribution of electrons, ions, and metastables, farther away from the axis and this variation in the number density distribution can be attributed to the fact that PIC/MCC simulations are kinetic while Shneider *et al.*[4] uses

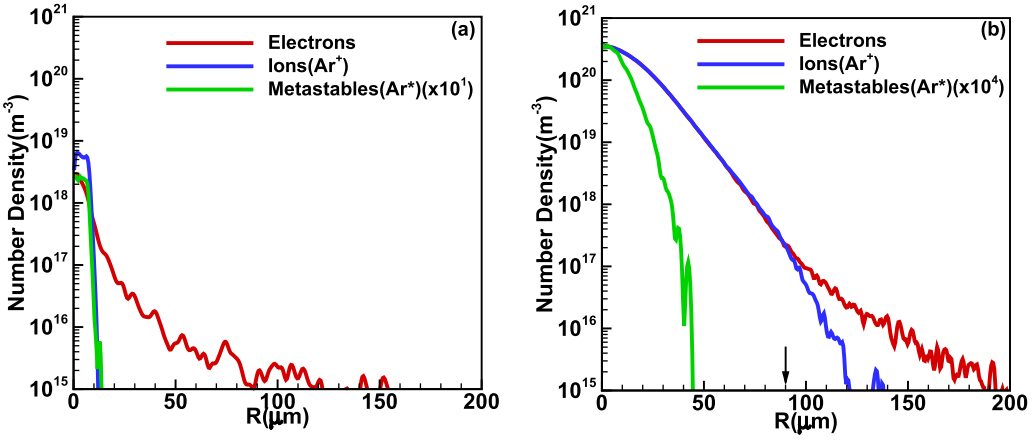

FIG. 4. Plasma expansion at (a) t = 0 ns and (b) t = 50 ns, showing free diffusion and ambipolar diffusion with arrow representing the bound of quasi-neutral plasma.

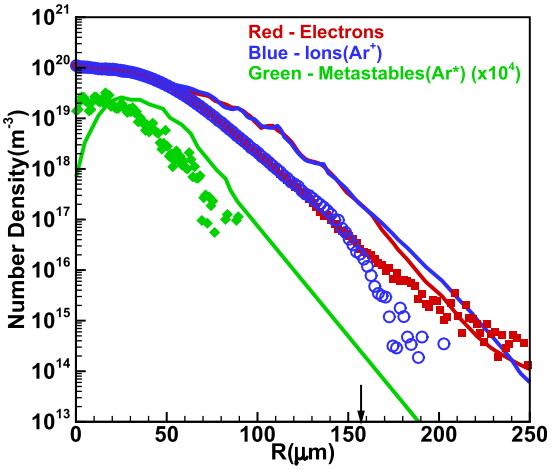

FIG. 5. Comparison of radial distribution of number densities from PIC/MCC and from drift diffusion approximation[4] at t = 100 ns with the arrow representing the bound of quasi-neutral plasma. PIC/MCC simulation results are represented by symbols and drift diffusion approximation results[4] are represented by lines.

a fluid approximation. The former factors in various aspects of the process in addition to the latter as described in Sec. II.

Figure 6 shows a comparison of the electron temperature at the core of the laser focus between PIC/MCC simulations and drift diffusion approximation.[4] The temperatures tend to the same value (≈0.65 eV) as time progresses. For PIC/MCC simulations, a peak in electron temperature of $T_e \approx 2.2$ eV could be observed at approximately 10 ns, which precedes the peak in the laser pulse occurring at about 20 ns. During the laser pulse, the electron energy distribution is highly non-equilibrium. The electron temperature at the core is a weighted average of the temperature of "hot" and "cold" electrons. The "hot" electrons are those that had just been generated by the laser pulse. The cold electrons are those that had already been scattered by the gas. Note that the mean time for an electron to undergo an elastic collision with an Argon neutral is $\tau_m = 37.7$ ps.[12] The electron temperature reaches a peak when the fraction of hot electrons is at a maximum. It can also be observed that this trend continues until the start of ambipolar diffusion. In contrast, the drift-diffusion approximation corresponds to a single temperature Maxwell-Boltzmann distribution and yields a monotonously decreasing electron temperature. There is also heating of the gas due to the electron energy relaxation in collisions with gas particles and transfer of the kinetic energy of the electrons and ions to the gas during the ambipolar expansion, but it decreases with time and the gas at the core reaches a temperature increase in the order of 10 K, which is in agreement with Shneider *et al.*[3]

A comparison of the electron energy distribution function (EEDF) from PIC/MCC simulation and Maxwell-Boltzmann energy distribution for the same mean energy near the axis at different time instants is shown in Fig. 7. At t = 10 ns, it can be observed that there is a significant fraction of electrons that are both accelerated and decelerated from their initial energy of 3.2 eV. The decelerated electrons are those that diffuse radially outward and are decelerated by the polarization field, while the accelerated electrons are those that have a radial velocity towards the axis and hence are accelerated by the polarization field. Figure 7 also shows the qualitative deviation of the EEDF from Maxwell-Boltzmann for the same mean energy, and it is higher for t = 10 ns than at t = 100 ns, since, as time progresses, the EEDF from PIC/MCC tends towards Maxwell-Boltzmann distribution.

The deviation of the EEDF from Maxwell-Boltzmann distribution is quantified in terms of a parameter, f_{max}^{eq} given by

$$f_{max}^{eq}(\%) = \left[\frac{\left(\frac{\Delta N}{N}\right)_{PIC/MCC,\varepsilon 1}}{\left(\frac{\Delta N}{N}\right)_{Boltzmann,\varepsilon 1}} - 1 \right] \times 100, \qquad (8)$$

where N is the total number of electrons, $\varepsilon 1$ is the energy that corresponds to the maximum value of $(\Delta N/N)_{PIC/MCC}$ for a given mean energy ($\bar{\varepsilon}$) in the EEDF, and $(\Delta N/N)_{Boltzmann,\varepsilon 1}$ is the fraction of electrons from the Maxwell-Boltzmann energy

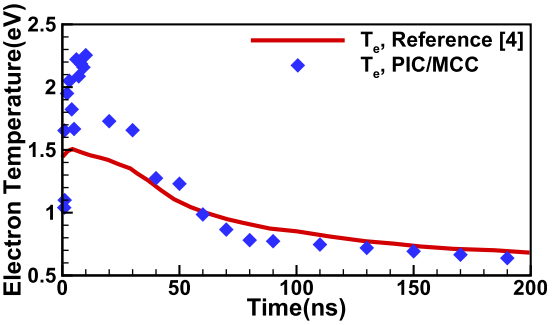

FIG. 6. Comparison of time evolution of electron temperature at the core of the laser focus from PIC/MCC and from drift diffusion approximation at the axis.[4]

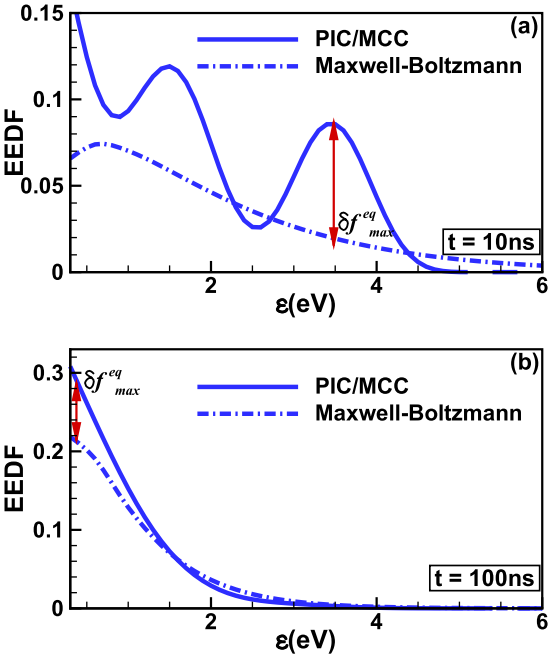

FIG. 7. Comparison of EEDF between PIC/MCC and Maxwell-Boltzmann of the same mean energy at R = 2 μm from PIC/MCC at (a) t = 10 ns and (b) t = 100 ns.

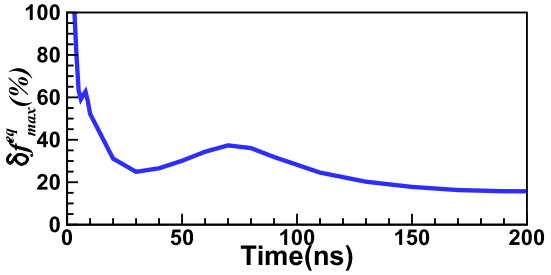

FIG. 8. Maximum deviation of EEDF from PIC/MCC to that of Maxwell-Boltzmann for the same mean energy.

distribution (constructed based on the mean energy of electrons ($\bar{\varepsilon}$) from the simulation) that have the energy, $\varepsilon 1$. The maximum deviation of EEDF from Maxwell-Boltzmann distribution is shown in Fig. 8. Figure 8 clearly shows that the electrons tend to equilibrium as time progresses, as the maximum deviation of EEDF (PIC/MCC) from Maxwell-Boltzmann tends to a small constant value of about 15%.

Considering mean energy is directly proportional to mean temperature, Fig. 9 shows the temporal evolution of the electron temperature at $R = 2\,\mu$m. Till 10 ns from the start of the pulse, i.e., t = 0 s, the Debye radius, $\lambda_D \approx 6\,\mu$m at $R = 2\,\mu$m, and the plasma radius, R_p, do not cross $6\,\mu$m till t = 3 ns. Since $\lambda_D > R$ till t = 3 ns, the dominant diffusion process is free diffusion. At t ≈ 3 ns, the Debye radius, $\lambda_D \approx 6\,\mu$m and plasma radius, $R_p \approx 7.5\,\mu$m, hence $\lambda_D < R_p$ indicating ambipolar diffusion. Hence, the time zone- *Free Diffusion* is predominantly characterized by pure (free) electron diffusion. There is a drop in mean energy at t ≈ 7.5 ps which is equal to the time taken by the electrons to travel across the initial plasma core, i.e., t = (7.5 [μm]/v_e [m/s]) ≈ 7.5 ps. The increase in the mean energy near the axis can be attributed to the acceleration of electrons with a negative radial velocity due to the polarization field. The time zone- *Ambipolar Expansion* is predominantly characterized by unsteady ambipolar expansion and hence the decrease in the mean energy.

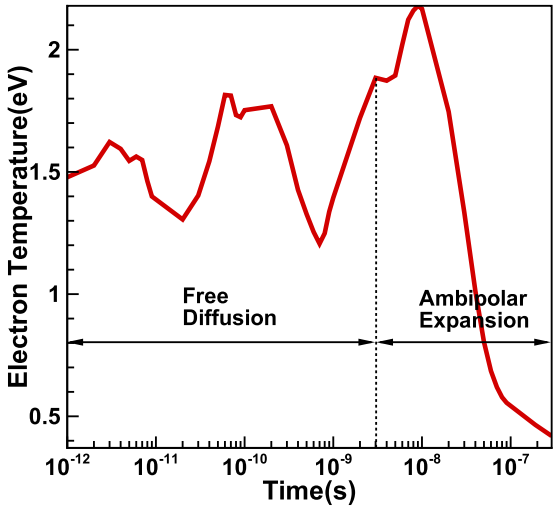

FIG. 9. Electron temperature evolution with time, near the axis ($R = 2\,\mu$m).

B. 2D approximation

The number density contours of electrons and ions at different instants in time are shown in Fig. 10. Figures 10(a)–10(c) clearly indicate the presence of the quasi-neutral plasma region in the shape of an ellipse in the R-Z plane.

Figures 10(a)–10(c) also show that a fraction of electrons are outside the quasi-neutral plasma and free diffusion is the process of their expansion. At the same time, the

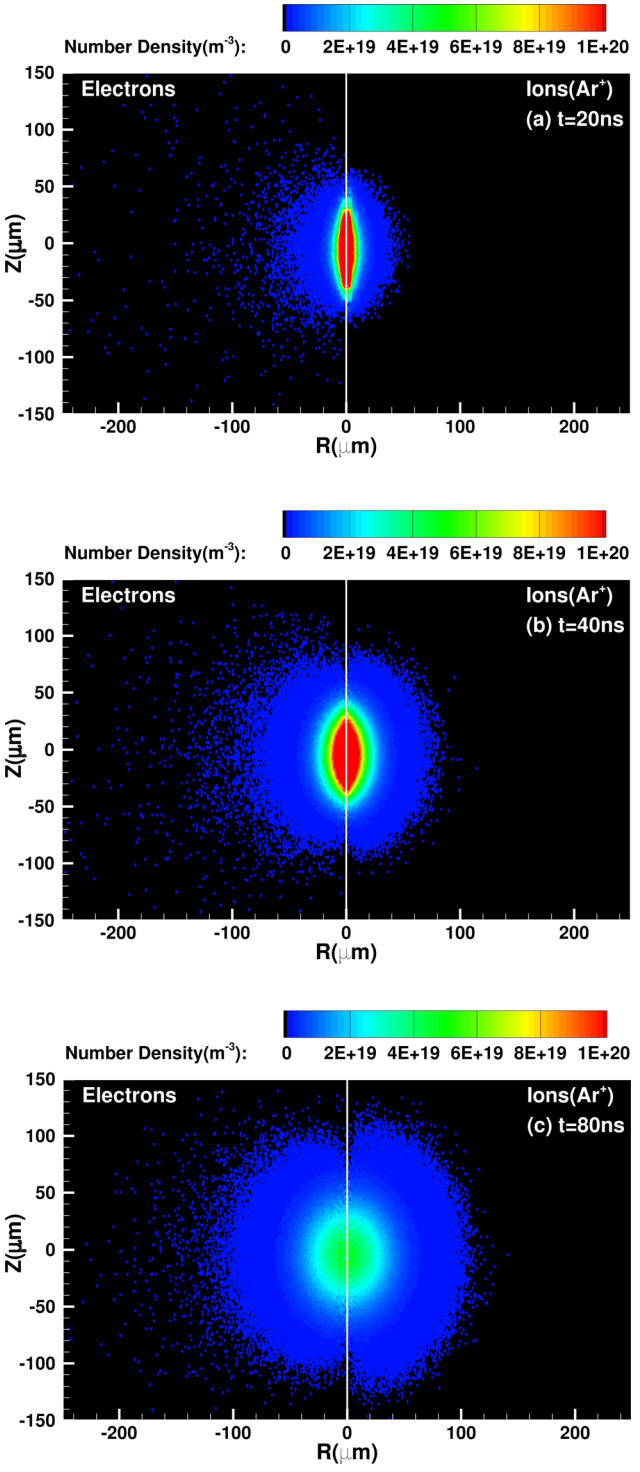

FIG. 10. Evolution of plasma with time: (a) t = 20 ns (AR = 1.45), (b) t = 40 ns (AR = 1.15), and (c) t = 80 ns (AR = 1.02) from 2D approximation.

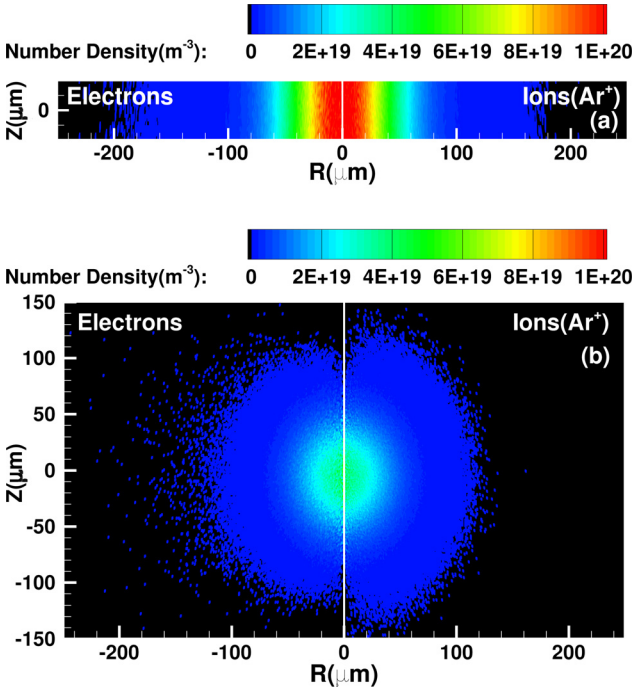

FIG. 11. Comparison of electron and ion number densities at t = 100 ns between (a) 1D approximation and (b) 2D approximation (AR = 1.02).

clear expansion of the ions and electrons together from Figs. 10(a) to 10(c) indicates ambipolar diffusion. A fraction of ions can be seen outside the plasma, which in a way represent the cathode fall region.[14]

One of the key results from the 2D simulations, is the comparison of the extents of axial and radial expansion. This can be analyzed based on the variation of aspect ratio (AR) of the ellipse in the R-Z plane with time. Hence, in this case, the AR of the expanding plasma is defined as the ratio of the axial length of the plasma to twice the radial length of the plasma. The aspect ratio of the plasma decreases from 5 to 1.02 in 100 ns, indicating a broadening of the ellipsoidal plasma region towards a spherical one. Hence, a significant axial expansion is present, indicating the importance of the 2D effects.

A comparison of the number densities of electrons and ions at t = 100 ns is shown in Fig. 11. It could be clearly seen that the plasma has expanded in both the radial and axial directions. Note that the relative expansion in the axial direction ($\Delta z/z_0 \approx 115/100 = 1.15$) is an order of magnitude smaller than that in the radial ($\Delta r/r_0 \approx 97.5/7.5 = 13$). The number density comparison in Fig. 11 also shows higher densities near the axis in 1D than in 2D, because the axial expansion is not accounted for in 1D. A region similar to the cathode fall with more number of ions, in glow discharges is observed in the REMPI plasma expansion process at the boundary of the plasma both in 1D and 2D, because of the lower number of electrons (due to the loss of electrons by

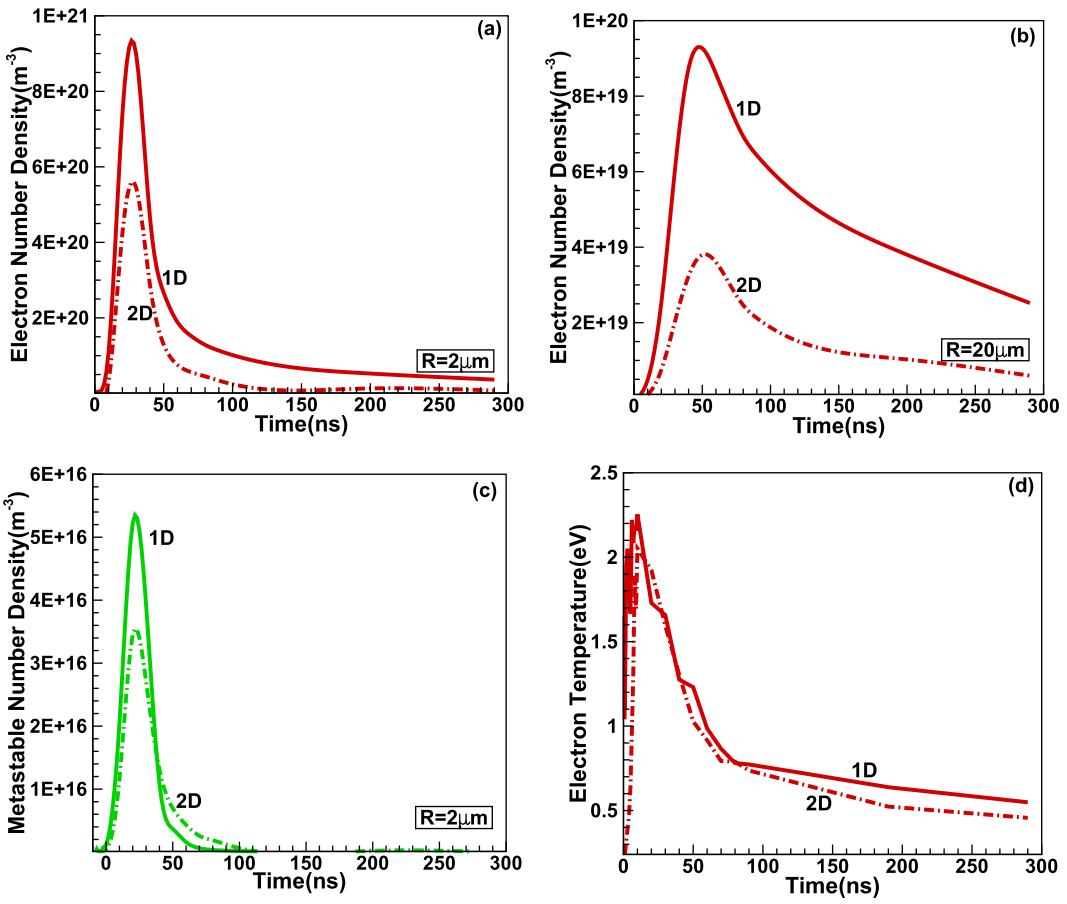

FIG. 12. Comparison of time evolution in 1D and 2D of: (a) electron number density at R = 2 μm, (b) electron number density at R = 20 μm, (c) metastable number densities at R = 2 μm, and (d) electron temperature at the core of the laser pulse averaged over a region from Z = −1 μm to Z = 1 μm.

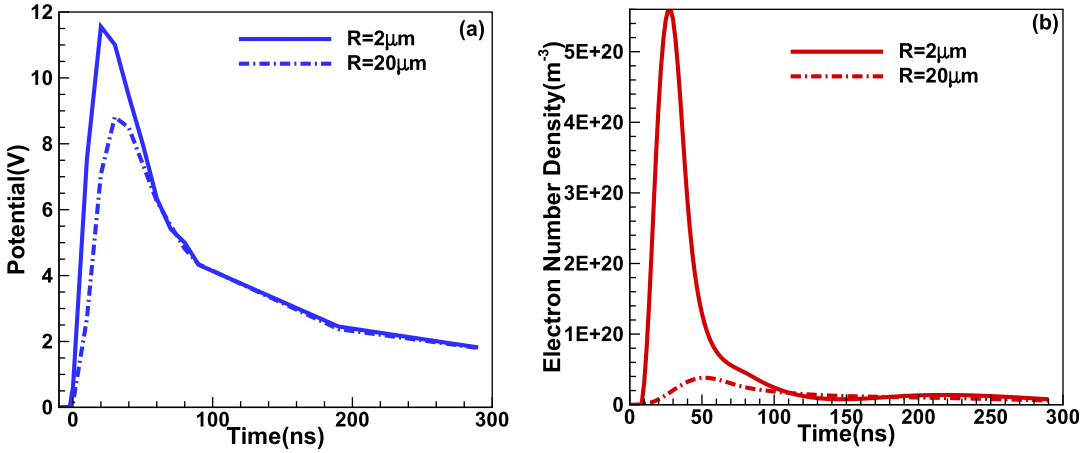

FIG. 13. Time evolution of (a) electric potential and (b) electron number density at R = 2 μm and R = 20 μm averaged over a region from Z = −1 μm to Z = 1 μm for 2D approximation.

free diffusion) as is observed by the number density contours of electrons and ions in Fig. 11(b).

Figures 12(a)–12(c) show the number density comparison of multiple species involved in the expansion process for 1D and 2D approximations near the axis. Up to t = 20 ns, i.e., 30 ns from the start of the laser pulse, the electron and metastable number densities for the 2D approximation follow the 1D approximation very closely and then it starts to diverge from 1D approximation. It can be observed that the 1D approximation predicts 1.5 to 2 times the 2D approximation values of the number densities from Figs. 12(a)–12(c), since the REMPI expansion process is both radially and axially dependent in 2D approximation, while it is only radially dependent in 1D approximation and, hence, the relaxing effect as has been explained earlier with the help of the expanding plasma's aspect ratio. The temporal evolution of ion number densities near the axis is same as that of the electrons (as it is in the plasma core). Fig. 12(b) has a higher deviation in the electron number densities than that of Fig. 12(a) initially because the electrons in that region are governed by free diffusion till then. Fig. 12(d) shows a comparison of electron temperature in 1D and 2D at the core of the laser pulse for 1D and 2D approximations, and it can be observed that the electron temperature for 2D is approximately 15% lower than the 1D approximation.

Temporal evolution of potential shown in Fig. 13(a), indicates a peak in potential in the first few nanoseconds, both at $R = 2\ \mu$m and $R = 20\ \mu$m and then a monotonous decrease due to ambipolar diffusion. Fig. 13(b) shows the temporal evolution of electron number density for 2D approximation at $R = 2\ \mu$m and $R = 20\ \mu$m averaged over a region from $Z = -1\ \mu$m to $Z = 1\ \mu$m, and as expected, the peak in the electron number density is higher near the axis, due the inverse exponential dependence of laser intensity with the radius which leads to a higher amount of plasma generation towards the axis. The electron number density both at $R = 2\ \mu$m and $R = 20\ \mu$m tends to approximately the same value as time progresses as shown in Fig. 13(b).

In this case, the microwave radiation wavelength is much higher than the plasma dimensions, and the skin layer exceeds the plasma scale, and all plasma electrons are oscillating in the same phase, the microwave scattering by the micro-plasma occurs in the Rayleigh mode.[3,4,13] Wherein the intensity of the scattered microwave radiation, $I_m \sim N_e^2$ and therefore, the amplitude of the electric field, measured by homodyne detection, $E_m \sim N_e(t)$.[3,4] A comparison of the normalized total number of electrons between 1D PIC/MCC, 2D PIC/MCC, and Shneider *et al.*,[4] theory and microwave scattering signal from experiments is shown in Fig. 14. The results in Fig. 14 show that PIC/MCC computations are in good agreement with the experiments. The PIC/MCC simulation results follow the drift diffusion approximation[4] till t = 110 ns, but PIC/MCC simulation results closely follow the experiments.

V. CONCLUSIONS

A computational model for REMPI plasma expansion of Argon gas at low pressures, using PIC/MCC both in 1D and 2D, has been presented. The results of calculations within the PIC/MCC and diffusion-drift approximations are in qualitative and in reasonable quantitative agreement. All stages of the ambipolar diffusion have been captured in the simulations. In spite of the fact that the 2D and 1D calculations are qualitatively consistent with each other, the two-dimensional

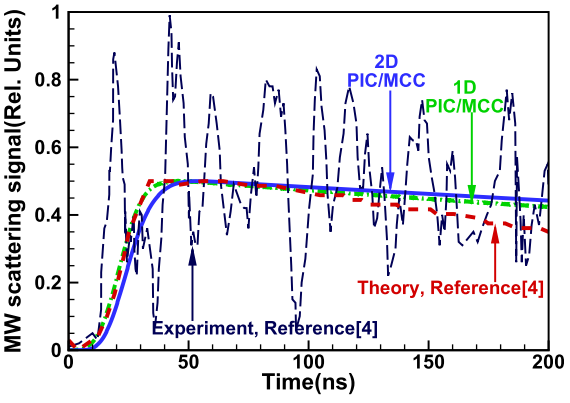

FIG. 14. Comparison of the scattering microwave signal from experiment from Shneider *et al.*[4] with 1D fluid approximation from Shneider *et al.*,[4] 1D PIC/MCC and 2D PIC/MCC for 3 + 1:REMPI of Ar gas at p = 5 Torr, with a laser pulse of 261.27 nm wavelength and $E = 2.1$ mJ/pulse.

effects are important, as the calculations showed a significant quantitative difference of the plasma characteristics, growing with time. It can be concluded that the polarization field plays a very important role in the relaxation of the electrons. The deviation of EEDF from the Maxwell-Boltzmann energy distribution has been qualitatively shown. A clear demarcation of the physical phenomena that are predominant at different instances of time has been identified.

Even for an elongated ellipsoid REMPI, which behaves as 1D plasma initially, over time evolves to a faster 2D spherical ambipolar plasma expansion with a significantly lower electron temperature and, therefore, more intense recombination processes. The PIC/MCC model follows the experimental measurements more closely than the drift diffusion approximation. Application of PIC/MCC, allows to resolve self-consistently, the problem of the microwave radiation scattering dynamics, taking into account the real phase changes of the electron oscillations in the microwave field.

ACKNOWLEDGMENTS

The development of extended plasma chemistry model in the PIC/MCC solver was partially supported by NSF ECCS Grant No. 1202095.

[1]R. Miles, Z. Zhang, S. Zaidi, and M. Shneider, AIAA J. **45**, 513 (2007).
[2]S. F. Adams, J. A. Miles, and A. Laber, in *48th AIAA Aerospace Sciences Meeting*, Orlando, Florida (AIAA, 2010), p. 87.
[3]Z. Zhang, M. N. Shneider, and R. B. Miles, Phys. Rev. Lett. **98**, 265005 (2007).
[4]M. N. Shneider, Z. Zhang, and R. B. Miles, J. Appl. Phys. **102**, 123103 (2007).
[5]F. H. M. Faisal, *Theory of Multiphoton Processes*, 1st ed. (Plenum Press, 1986).
[6]J. P. Verboncoeur, Plasma Phys. Controlled Fusion **47**, A231 (2005).
[7]*Reference Book on Constants of Elementary Processes with Atoms, Ions, Electrons and Photons*, edited by A. G. Zhiglinskii (Saint Petersburg State University, Saint Petersburg, Russia, 1994).
[8]Y.-J. Shiu and M. A. Biondi, Phys. Rev. A: At., Mol., Opt. Phys. **17**, 868 (1978).
[9]J. Stevefelt, J. Boulmer, and J. F. Delpech, Phys. Rev. A: At., Mol., Opt. Phys. **12**, 1246 (1975).
[10]V. Vahedi and M. Surendra, Comput. Phys. Commun. **87**, 179 (1995).
[11]J. Verboncoeur, A. Langdon, and N. Gladd, Comput. Phys. Commun. **87**, 199 (1995).
[12]Y. P. Raizer, *Gas Discharge Physics*, 1st ed. (Springer-Verlag, 1994).
[13]M. N. Shneider and R. B. Miles, J. Appl. Phys. **98**, 033301 (2005).
[14]A. Fridman and L. A. Kennedy, *Plasma Physics and Engineering*, 3rd ed. (CRC Press, 2011).
[15]C. K. Birdsall, *Plasma Physics via Computer Simulation*, 1st ed. (CRC Press, 1991).
[16]G. A. Bird, *Molecular Gas Dynamics and the Simulation of Gas Flows*, 1st ed. (Clarendon Press, 1991).